

Controlling the electronic interface properties of $\text{AlO}_x/\text{SrTiO}_3$ heterostructures

Berengar Leikert,¹ Judith Gabel,^{1,2} Matthias Schmitt,¹ Martin Stübinger,¹ Philipp Scheiderer,¹ Louis Veyrat,¹ Tien-Lin Lee,² Michael Sing,¹ and Ralph Claessen¹

¹*Physikalisches Institut and Würzburg-Dresden Cluster of Excellence *ct.qmat*,
Universität Würzburg, D-97074 Würzburg, Germany*

²*Diamond Light Source, Harwell Science and Innovation Campus, Didcot, OX11 0DE, UK*

(Dated: April 14, 2021)

Depositing disordered Al on top of SrTiO_3 is a cheap and easy way to create a two-dimensional electron system in the SrTiO_3 surface layers. To facilitate future device applications we passivate the heterostructure by a disordered LaAlO_3 capping layer to study the electronic properties by complementary x-ray photoemission spectroscopy and transport measurements on the very same samples. We also tune the electronic interface properties by adjusting the oxygen pressure during film growth.

I. INTRODUCTION

The famous high-mobility two-dimensional electron system (2DES) at the epitaxial interface of the band insulators SrTiO_3 (STO) and LaAlO_3 (LAO)[1] with its multiple intriguing electronic properties such as superconductivity, magnetism and even the coexistence of both [2] has sparked intense interest in transition-metal oxide heterostructures. [3–6]. These materials and the LAO/STO 2DES in particular are a fascinating wellspring for novel functionalities, for example in memresistive devices [7]. However, heterostructuring with epitaxial LAO layers is not the only way to create a 2DES in STO. It can also be generated, e.g., by capping with disordered LAO (d-LAO) [8] or by irradiation with intense synchrotron light [9, 10]. A particular interesting route was recently reported by Rödel *et al.* [11], who use a very simple and easily upscalable approach, namely room-temperature evaporation of Al on a STO surface. This results in a disordered and partially oxidized Al film, where the oxygen is scavenged from the STO creating O vacancies near the surface which in turn act as *n*-dopants and thus give rise to the 2DES. Their *in situ* angle-resolved photoemission spectroscopy (ARPES) data shows that just about one monolayer of Al suffices to create a 2DES.

The system AlO_x/STO has been studied also by other groups. Fu and Wagner [12] evaporated 6 nm of Al on top of STO and analyzed the Al oxidation state by x-ray photoemission spectroscopy (XPS) as function of annealing temperature after film deposition. They observed partial oxidation of the Al layer even at room temperature and strongly enhanced oxidation upon further annealing. In another XPS study on multiple metal/STO interfaces Posadas *et al.* [13] focused on the role various material parameters play for 2DES formation, namely the work-function difference between metal and STO as well as the heat of formation for metal oxide versus oxygen vacancies in STO. They confirm that the redox reaction between Al and the STO surface saturates after about one monolayer of deposited Al, with the resulting metallicity of the STO surface indicated by a shoulder of reduced Ti^{3+} in the $\text{Ti } 2p$ spectrum. Very recently, Vicente-Arche *et al.* also observed a reduction of the STO surface layers upon

depositing various metals, amongst them Al, in photoemission spectroscopy [14]. They also confirm that the interfacial redox reaction saturates after a certain metal thickness and observe metallic behavior in *ex situ* transport measurements.

Several other groups have studied quantum transport in the AlO_x/STO system. For example, Sengupta *et al.* [15] confirmed metallicity and even studied the superconducting regime of the 2DES by application of gate voltages and magnetic fields. Wolff *et al.* [16] reported transport experiments on AlO_x/STO samples grown by pulsed laser deposition (PLD) using an Al_2O_3 target for film growth. This growth technique is, however, more complicated, less suitable for upscaling, and may affect the formation of the AlO_x/STO interface in a different way due the high kinetic energy ions in the PLD plasma plume. Vaz *et al.* [17] even went one step further by combining the AlO_x/STO interface with a NiFe layer for spin pumping experiments, thereby paving the way for novel oxide based spintronic devices.

We note that all of these transport experiments were performed *ex situ*, i.e., outside the vacuum of the growth chamber. Unfortunately, so far no systematic information has been provided how exposure to air might affect the pristine sample properties as probed in the aforementioned photoemission studies [18].

With this in mind and motivated by its intriguing simplicity we elaborate in this study on the fabrication of AlO_x/STO by thermal Al evaporation. We develop a reliable passivation layer for the heterostructure enabling the direct correlation of *in situ* photoemission spectroscopy and *ex situ* electrical transport measurements on the same device-like samples. By combining the results of both techniques we demonstrate how the growth parameters can be used to control the carrier density of the ensuing 2DES.

II. EXPERIMENTAL DETAILS

The STO substrates from Crystec GmbH were TiO_2 terminated as described elsewhere [19, 20]. Immediately before the Al growth they were annealed inside a vacuum chamber at 500°C in a 1×10^{-5} mbar O_2 atmo-

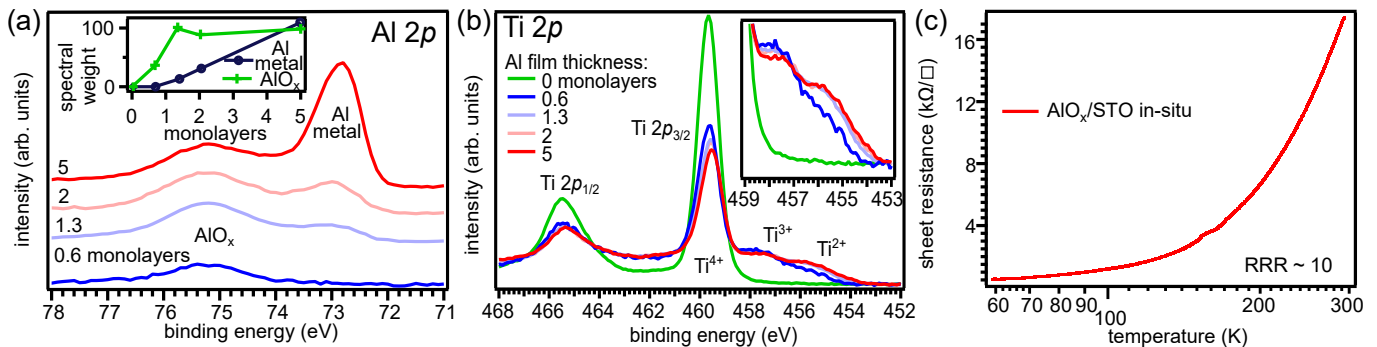


FIG. 1. (a) Al $2p$ spectra dependent on film thickness. The spectra are offset for clarity and normalized to integral Ti $3s$ spectral weight. The inset shows the spectral weight of the features as function of film thickness. (b) Ti $2p$ spectra of the samples in (a) at the corresponding Al film thicknesses in contrast to the Ti $2p$ spectrum of bare Nb:STO. The significant, chemically shifted Ti^{3+} and Ti^{2+} features, developing upon Al deposition, indicate the formation of oxygen vacancies, which dope the STO with electrons. The reduction of Ti saturates at the same film thickness as the Al oxidation. The spectra are normalized to integral Ti $2p$ spectral weight. (c) Temperature dependent sheet resistance of a sample with an Al film thickness of 5 nm. The red curve corresponds to a measurement before exposure to air, i.e., it was recorded *in situ*. It shows metallic behavior with a residual resistivity ratio (RRR) of about 10, while the resistance of the sample was beyond the measurement limit after exposure to ambient conditions, i.e., when measured *ex situ*.

sphere. After the substrates had cooled down to room temperature, aluminum was deposited by thermal evaporation from an effusion cell, in ultrahigh vacuum (UHV) or under various oxygen background pressures. The film thicknesses were derived by monitoring the evaporation rate with a quartz microbalance and calibrating the flux against x-ray reflectivity data measured for of a thick Al film grown on STO. After growth the samples were transferred *in situ* into a photoemission chamber and characterized by XPS, using a monochromated Al K_{α} x-ray source and an Omicron EA-125 spectrometer. Before the samples were removed from vacuum for the *ex situ* transport experiments, they were capped by 3 nm of disordered LAO. This was achieved after another *in situ* transfer into a dedicated UHV chamber for pulsed-laser deposition. The disordered LAO films were ablated from a single crystal target at room temperature, with a laser flux of 1.3 J cm^{-2} , a pulse frequency of 1 Hz, a target-substrate distance of 5 cm and *in vacuo*. In order to establish that the capping does not alter the spectroscopic properties of the films the passivated samples were probed by hard x-ray photoelectron spectroscopy (HAXPES) at beamline I09 of the Diamond Light Source (UK), using a photon energy of $h\nu = 3 \text{ keV}$ and a sample temperature of 50 K.

Transport measurements of the passivated samples were performed in a Physical Property Measurement System (PPMS) by Quantum Design. For these experiments the samples were contacted by ultrasonic Al wire bonding in van der Pauw geometry. Longitudinal and Hall resistance was measured in a temperature range between 2 K and 300 K and at magnetic fields up to $\pm 9 \text{ T}$ perpendicular to the sample surface. A small set of samples was also mounted insulating on a dedicated sample holder and contacted before growth to enable *in situ* transport experiments for comparison.

III. EXPERIMENTAL RESULTS

A. XPS analysis of pristine AlO_x/STO

We begin by calibrating our pristine AlO_x/STO films grown in UHV, i.e., without any additional oxygen supply, against the results of previous studies in the literature, using XPS as spectroscopic characterization tool. For this purpose we show in Fig. 1(a) the Al $2p$ spectrum as function of film thickness. Starting with the lowest Al coverage (nominally corresponding to 0.6 monolayers) we observe a single peak at 75.2 eV binding energy which is the value expected for fully oxidized Al [21]. With increasing coverage an additional and chemically shifted component at 72.8 eV can be seen to develop. It is readily identified as due to metallic Al [21] and strongly increases in spectral weight relative to the oxide peak upon further evaporation. This behavior is fully consistent with the observations of Rödel *et al.* [11]. In the absence of other oxygen sources these spectra strongly suggest that the first Al atoms deposited on the substrate surface become oxidized to AlO_x (mostly Al_2O_3) by scavenging oxygen from the top STO layers. Interestingly, the intensity of the AlO_x peak remains rather constant for increasing Al coverages [cf. inset Fig. 1(a)], indicating that the redox process saturates already after one monolayer while all additional Al stays in a metallic state.

Independent evidence that the oxidation of the first Al layer creates oxygen vacancies near the AlO_x/STO interface is provided by the Ti $2p$ spectrum [see Fig. 1(b)]. While the bare substrate displays only a single Ti^{4+} peak, we detect additional Ti^{3+} and Ti^{2+} signals [21] upon Al deposition, best observed on the lower binding energy side of the Ti $2p_{3/2}$ peak. The reduced Ti valences are a fingerprint of the formation of single or even clustered oxygen vacancies (in the case of Ti^{2+}) on the STO side of the interface [22]. The relative intensity of these peaks

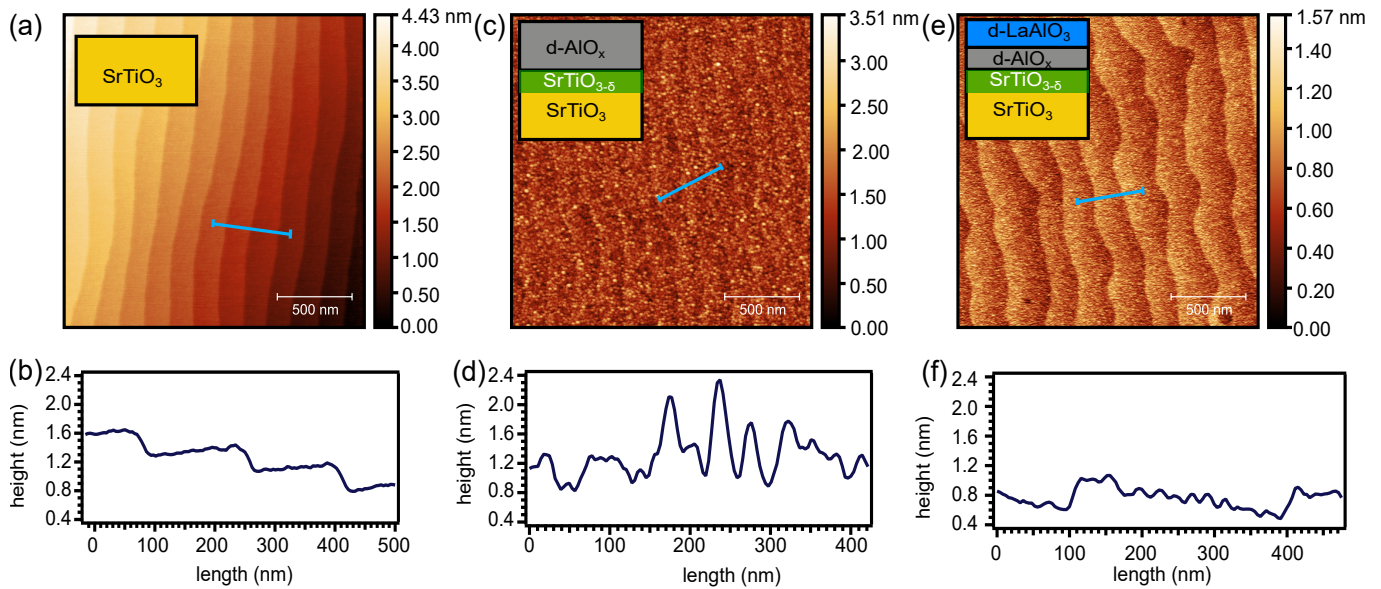


FIG. 2. (a) AFM image of an etched, TiO_2 terminated STO substrate displaying large, flat terraces. (b) Profile along the line indicated in (a). The steps between the terraces are 0.4 nm high, corresponding to one STO unit cell. (c) AFM image of a nominally 5 nm thick, disordered AlO_x film on top of a STO substrate. Terraces, as imposed by the substrate, are barely seen. Rather large AlO_x clusters are formed which appear as peaks with steep slopes in AFM line profiles. An example is shown in (d) along the line indicated in (c). The peak heights amount to over 1 nm. (e) AFM image of 3 nm d-LAO on top of nominally 2 nm AlO_x on STO [total nominal film thickness of 5 nm as in (c)]. Terraces are clearly distinguishable. The film roughness is smaller than in (c). (f) Profile along the line in (e).

with respect to that of the tetravalent, i.e., fully oxidized, Ti species displays very little change for Al coverages above one monolayer, again pointing to a saturation of the interfacial redox reaction.

The oxygen vacancies thus act as n -dopants which donate electrons to the STO conduction band states near the interface, thereby forming the 2DES [13, 23–26], as is demonstrated by the temperature-dependent resistivity curve in Fig. 1(c) for a nominally 5 nm thick AlO_x film. Note that this resistivity data has been measured *in situ* by using a special set-up in our vacuum system that avoids exposure of the sample to atmosphere. Due to experimental limitations our *in situ* resistivity measurements could not access the temperature range below 60 K. After exposing the film intentionally to ambient conditions, the sheet carrier resistance was beyond the measurement limit.

B. Surface passivation

For a more systematic transport characterization, going down to liquid helium temperatures and including also the measurement of the Hall resistivity, we had to take the samples out of the vacuum in order to transfer them to our PPMS. For such *ex situ* experiments it is of paramount importance that air exposure does not cause the created oxygen vacancies to become refilled again. Indeed, all our films with nominal thicknesses up to 5 nm were found to become insulating upon exposure to air. We attribute this to their higher surface roughness

compared to the bare substrate, as seen in the atomic force microscopy (AFM) images of an STO sample before and after Al deposition in Fig. 2(a)-(d). While the bare substrate terraces are still atomically flat, the AlO_x film shows substantial surface corrugations on the scale of 1 nm or more. This implies that between thicker AlO_x grains the film may become too thin to prevent oxygen diffusion into the STO. As a result, oxygen atoms refill the vacancies which eventually renders the samples insulating.

One possible solution to this problem could be the use of thicker Al films, utilizing the fact that Al develops a natural oxide layer of the order of 2 nm in air [27] which then can act as a protecting capping. While this approach seems to have worked well in previous studies [11, 14, 15], we found it problematic. On the one hand a passivation layer based on Al must not be too thin in order to suppress O diffusion to the substrate. If on the other hand the Al film is too thick, a metallic, i.e., conducting Al layer may form between the passivating surface oxide and the insulating AlO_x phase at the interface, which in transport measurements will shunt the response from the 2DES in the STO. This is indeed what we observed for many of our thicker Al films.

In search for a less critical passivation layer we discovered that disordered LAO (d-LAO), grown by room-temperature PLD on top of our AlO_x /STO films, is a viable option. Independent of its crystalline state (long-range ordered or disordered) and insensitive to slight variations in stoichiometry (controlled by the PLD growth parameters) it remains always insulating. Furthermore,

d-LAO not only prevents O-diffusion to the substrate, it also tends to stabilize the 2DES as it is known to induce O vacancies in STO by itself [28]. Deposition of the protecting d-LAO layer leads to a significant smoothening of the surface compared to the uncapped AlO_x films, as is depicted in Fig. 2(e,f) showing AFM data of a sample with nominally 2 nm AlO_x capped by 3 nm d-LAO.

In order to check the passivating power of the d-LAO capping layer we have performed *in situ* four point resistivity measurements once before exposure to air and once after keeping the sample two hours outside the vacuum chamber. Figure 3(a) demonstrates that the temperature dependent sheet resistance of the sample is not altered and the d-LAO film fully passivates the heterostructure. The film stays metallic down to low temperatures with residual resistivity ratios (RRR) of the order of 10.

C. Transport experiments

Besides the longitudinal sheet resistance we have also measured the temperature-dependent Hall resistance of the d-LAO passivated samples. For temperatures below 50 K the Hall effect shows a transition from a linear behavior to a non-linear S-shape. We interpret this behavior as a sign of multiband transport, which is well-known to happen in STO based electron gases [14, 29]. We fitted the nonlinear Hall effect curves using a simple 2-band model to determine the corresponding sheet carrier densities and carrier mobilities which are shown in Fig. 3(b) and (c) [30]. The model yields two electron-like carrier populations, one with large density ($n_2 \approx 2 \times 10^{14} \text{ cm}^{-2}$) and low mobility ($\mu_2 \approx 140 \text{ cm}^2 \text{ V}^{-1} \text{ s}^{-1}$) and one with much smaller density ($n_1 \approx 1 \times 10^{12} \text{ cm}^{-2}$) and a significantly larger mobility ($\mu_1 \approx 2000 \text{ cm}^2 \text{ V}^{-1} \text{ s}^{-1}$). These data also reveal that a sizable fraction of the mobile charge carriers get frozen out at low temperatures, which is also observed in other STO based systems where doping is dominated by the formation of oxygen vacancies [8, 15, 16, 31]. Interestingly, the measured sheet carrier densities are at all temperatures higher than in the AlO_x/STO heterostructures of Sengupta *et al.* [15] and the PLD-grown AlO_x/STO heterostructures of Wolff *et al.* [16], likely due to significantly higher oxygen vacancy concentrations in our samples.

While the carrier mobility, on the other hand, is limited at high temperatures by phonon scattering, it increases at lower temperatures due to phonon freeze-out and eventually the mobility of the majority carriers saturates around $140 \text{ cm}^2 \text{ V}^{-1} \text{ s}^{-1}$ at liquid helium temperatures where the carrier mobility is largely determined by impurity scattering [32]. The order of magnitude of the low temperature mobility of the majority carriers is comparable to the other aforementioned oxygen vacancy governed STO systems [8, 16, 31] but lower than in the samples of Sengupta *et al.* [15]. This is again attributed to a higher vacancy concentration in our samples, highlighting their dual role as dopants and as scattering centers.

In order to exclude that the measured conductivity

stems from metallic Al in the film, a control experiment was conducted in which the same film was deposited on DyScO_3 (DSO), another wide-gap transition-metal perovskite oxide insulator. In contrast to STO, in DSO the electronic charges introduced by doping with oxygen vacancies remain completely trapped, thereby preventing the formation of a metallic 2DES [33, 34]. Thus, conduction in AlO_x/DSO would be an indication of remaining metallic Al. Indeed, all our AlO_x/DSO heterostructures grown under identical conditions as the AlO_x/STO films stayed insulating, with resistances beyond the measurement limit of the PPMS. As metallic Al is even less likely to form in AlO_x/STO , where the redox reaction is stronger, than in AlO_x/DSO , this control experiment strongly goes in favor of a totally oxidized and insulating Al layer.

D. Growth control of the interface properties

For device applications it is desirable that the electronic interface properties can be tuned. This is achieved by varying the growth parameters, in particular the O_2 background pressure applied during Al deposition. For a systematic study we have grown a series of Al films with 2 nm nominal thickness in oxygen background pressures between 1×10^{-8} mbar and 1×10^{-5} mbar. These samples were then characterized by *in situ* XPS and *ex situ* transport measurements. Please note that all photoemission spectra were taken before capping with d-LAO, if not stated otherwise.

We begin our analysis with a survey of the $\text{Al}2p$ spectra depicted in Fig. 4(a). For comparison of their relative intensities they have been normalized to the integral spectral weight of the $\text{Ti}3s$ substrate core level (not shown). Note, however, that an error is involved here since due to oxidation, i.e., the incorporation of oxygen, the same amount of deposited Al will result in a larger film thickness and hence stronger damping of the substrate signals. Thus, the integrated intensity of the spectra in fact is increasingly overestimated with increasing oxygen pressure. The qualitative trends, however, are not affected by this normalization as will become clear from the following discussion of the spectra. For films grown at low oxygen pressures the spectra resemble the red spectrum in Fig. 1(a), consisting of a metallic Al signal and a weaker oxide component at higher binding energy. For higher oxygen background pressures, the metallic Al peak is observed to decrease in intensity, while the AlO_x peak grows until only the latter is detected, demonstrating that the Al gets considerably stronger oxidized if deposited under a higher oxygen pressure.

This conclusion is confirmed by the behavior of the $\text{O}1s$ spectra in Fig. 4(b). These spectra are normalized to the integrated intensity of the $\text{Ti}2p$ substrate signal, chosen for its energetic vicinity [cf. Fig. 4(c)]. As above, there is a certain quantitative error concomitant with this normalization that, however, does not affect the qualitative interpretation of the data. The peak at

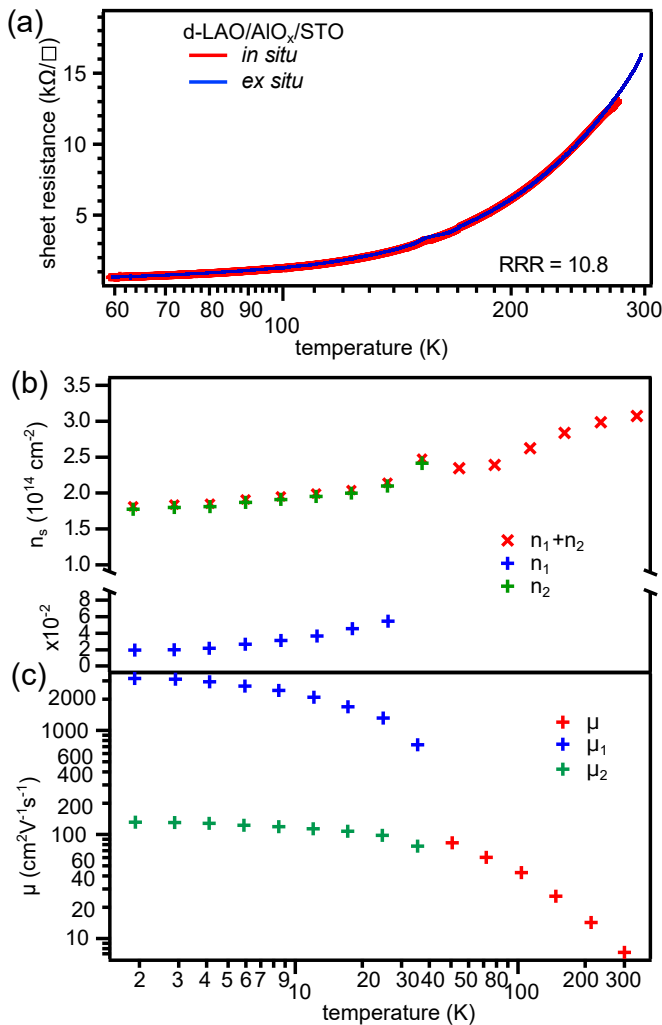


FIG. 3. (a) Temperature-dependent sheet resistance of a sample grown in vacuum with a 3 nm d-LAO capping of nominally 2 nm AlO_x on STO. The red curve depicts the sheet resistance of the sample before exposure to air, i.e., when measured *in situ*. Afterwards, the sample was taken out of the UHV cluster and kept in air for two hours, then the measurement was repeated *ex situ* (blue curve). The measurements agree with each other showing that the d-LAO capping layer successfully passivates the sample and enables *ex situ* sample transfer. (b) Red crosses: total sheet carrier density as function of temperature of a d-LAO/ AlO_x /STO sample (AlO_x grown in vacuum). At low temperatures, where the Hall resistance is non-linear, the total sheet carrier density consists of the sum of n_1 (blue crosses) and n_2 (green crosses), which were extracted from a 2-band fit [30]. (c) Corresponding mobility data as function of temperature.

531 eV is attributed to the oxygen in the STO substrate and stays approximately constant in intensity throughout the pressure series. For the lowest O_2 pressure an additional shoulder at 533 eV corresponding to oxygen in AlO_x is detected. With increasing oxygen background pressure it evolves into a pronounced peak that surpasses the substrate peak. Note that with the chosen normalization the spectral weight of the O 1s signal is a direct measure of the amount of oxygen in film and substrate,

respectively. The strong increase of the film component consequently signals that the increasing O_2 growth pressure leads to stronger oxygen incorporation into the AlO_x films.

So far we have seen that Al deposited on STO reacts both with oxygen diffusing out of the substrate as well as with O_2 supplied by the gas phase to form AlO_x . This raises the obvious question, if the latter route has an effect on the former, thereby influencing the generation of oxygen vacancies in the STO. This can be answered by XPS on the Ti 2p core level, as shown in Fig. 4(c). At low O_2 pressure, a huge Ti^{3+} shoulder and even a Ti^{2+} feature are observed in addition to the Ti^{4+} peak corresponding to stoichiometric STO. At higher oxygen background pressure the Ti^{3+} as well as the Ti^{2+} shoulders decrease in intensity, with the latter becoming even completely suppressed at the highest oxygen background pressure [s. inset of Fig. 4(c)]. We conclude that the strong oxidation resulting from evaporating Al in an oxygen atmosphere strongly reduces the scavenging of oxygen from STO, i.e., it reduces the oxygen vacancy concentration and thereby the n -doping of the interface layers.

Before we test this conclusion further by *ex situ* transport experiments on capped samples, we first establish that the spectroscopic information discussed above is not altered by the application of a passivating d-LAO capping. For this purpose we have employed *hard* x-ray photoelectron spectroscopy (HAXPES) at a photon energy of $h\nu = 3 \text{ keV}$, making use of the considerably enhanced probing depth compared to conventional XPS. This allows us to acquire a strong photoemission signal of the STO layers of passivated samples despite a total (nominal) film thickness of 5 nm (AlO_x and d-LAO). Figure 5(a) shows the Ti 2p core level spectra of a set of capped samples grown at different oxygen background pressures. Similar to the *in situ* XPS data on uncapped samples in Fig. 4(c) Ti^{2+} and Ti^{3+} features are clearly discernible in these spectra and become increasingly reduced in intensity for higher O_2 growth pressures.

Finally, our *ex situ* transport measurements confirm the metallic character of all samples regardless of the oxygen background pressure applied during growth. Figure 5(b) compiles the transport data for all samples, specifically the carrier density extracted from the Hall effect and the low-temperature mobility. The red curve depicts the sheet carrier density at 300 K, the same temperature at which the XPS experiments were performed, while the green curve is sheet carrier density at 50 K, where the HAXPES spectra were taken. The consistently lower carrier concentration at lower temperatures is due to the carrier freeze out already seen in Fig. 3(b). The sheet carrier density in both curves confirms the qualitative observations from the photoemission experiments in Fig. 4 and Fig. 5(a), namely a clear reduction with increasing O_2 growth pressure. It should be noted here that the metallic Al seen in the XPS spectra of Fig. 5(a) for samples grown at the two lowest O_2 pressures apparently does not form a percolative path shunting the conducting 2DES because otherwise the charge carrier concen-

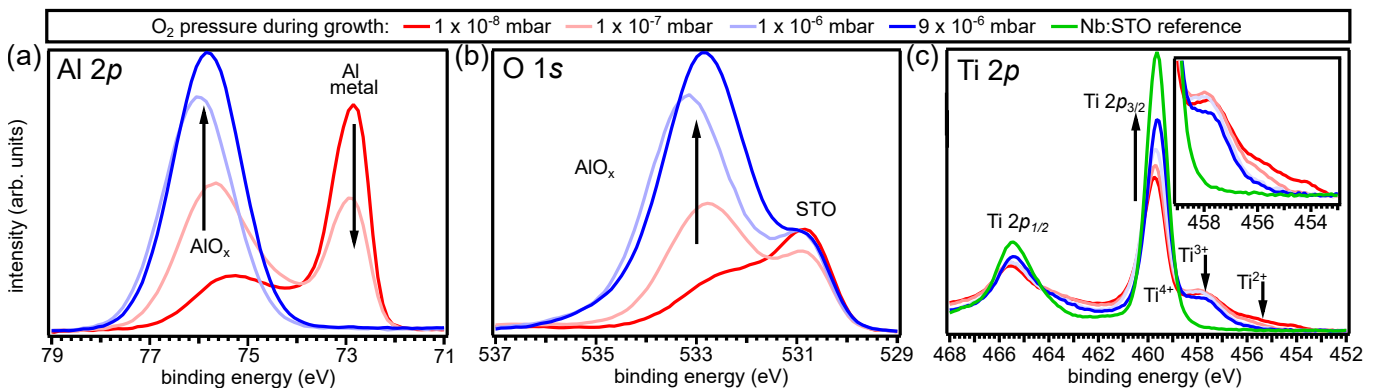


FIG. 4. XPS core level spectra dependent on the O_2 pressure during Al deposition. (a) $Al\ 2p$ spectra. With higher oxygen background pressure the metallic Al component shrinks while the AlO_x component grows. The $Al\ 2p$ spectra are normalized to the $Ti\ 3s$ spectral weight. (b) $O\ 1s$ spectra of the samples in (a) normalized to the $Ti\ 2p$ spectral weight. (c) $Ti\ 2p$ spectra of the same samples, normalized to integral $Ti\ 2p$ spectral weight. Besides the Ti^{4+} component of stoichiometric STO also a chemically shifted Ti^{3+} component, indicating the existence of oxygen vacancies, is detected. For samples grown in low oxygen pressures, also a sizable Ti^{2+} component is observed, suggesting even stronger reduction of the STO surface. With higher oxygen growth pressures the Ti^{2+} component vanishes and the Ti^{3+} component shrinks, while the Ti^{4+} component grows, showing that less oxygen vacancies are created.

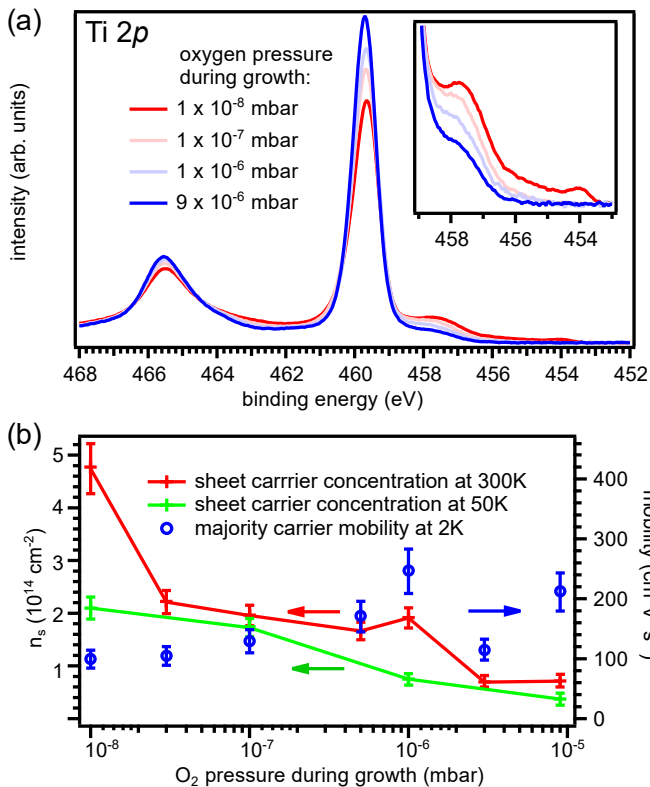


FIG. 5. (a) Hard x-ray photoemission $Ti\ 2p$ spectra ($h\nu = 3\text{ keV}$) of *ex situ* d-LAO/ AlO_x /STO samples where the Al was deposited at various O_2 pressures. Inset: Zoom-in on the low binding energy side of the $Ti\ 2p_{3/2}$ peak. (b) Left axis, red crosses: Sheet carrier concentration at 300K dependent on O_2 growth pressure. The line is a guide to the eye. Upon increasing the oxygen pressure during growth, the sheet carrier density decreases. Left axis, green crosses: Sheet carrier density at 50K. Right axis, blue circles: Mobility of the majority carriers at 2K dependent on O_2 pressure during growth. It displays no systematic behavior.

trations are expected to be much higher.

In contrast to the carrier concentration we do not observe any systematic dependence of the low-temperature mobility on oxygen background pressure [blue symbols in Fig. 5(b)]. This may either result from impurity scattering other than by the oxygen vacancies or indicate that the effective scattering rate is not only controlled by the concentration but also by the spatial depth profile of the vacancies. We will return to this point in the following section.

IV. DISCUSSION

In the first place, our combined photoemission and transport data clearly confirms that the 2DES formation in AlO_x /STO results from a redox process between the Al film and the substrate, generating *n*-doping oxygen vacancies in the STO. This mechanism is different from the generic electronic reconstruction scenario discussed for all-crystalline oxide heterostructures with a polar discontinuity like LAO/STO [1] or γ - Al_2O_3 /STO [4]. Note, however, that oxygen vacancy formation can also occur in those systems, substantially contributing to the carrier concentration of their 2DES and making their interface properties sensitive to the specific oxygen exposure during and even after epitaxial growth [25, 35]. This is exactly what we see here as well. The simplicity of the deposition process in the case of our AlO_x films provides us with the unique opportunity to control the working point of the redox reaction by supplying additional oxygen in the gas phase. This opens a second channel for aluminum oxidation, resulting in reduced formation of oxygen vacancies and hence a smaller sheet carrier density. Whether this effect is due to enhanced oxidation of the Al atoms during film growth (before or after deposition), thereby suppressing the scavenging of oxygen from

the substrate, or whether the background pressure leads to oxygen diffusion into the substrate and direct filling of the vacancies, cannot be decided on the data at hand. However, the fact that all of our uncapped AlO_x/STO samples turned insulating upon exposure to ambient atmosphere, seems to indicate that the latter process is at least part of the story.

While on the one hand the O_2 growth pressure can thus be viewed as a useful control parameter for the interface properties, the extreme air sensitivity on the other hand would seem to prevent any practical *ex situ* use of the AlO_x/STO heterostructures, unless they are protected by a suitable passivation layer. One possible candidate for such a protecting capping is the native oxide of Al itself, as was used by Sengupta *et al.* as well as by Vicente-Arche *et al.* for their *ex situ* transport experiments [14, 15]. For this purpose they simply exposed their thick Al films to air to create an oxygen diffusion barrier. However, in contrast to our study, the Al-films of Sengupta *et al.* were grown at elevated substrate temperatures (100...200°C), resulting in a smoother Al surface and hence better defined oxide capping. The choice of room-temperature growth in our case was motivated by trying to suppress the leveling effect of temperature-enhanced oxygen diffusion when studying the impact of oxygen background pressure during growth. The drawback of this approach is our larger film roughness (at same nominal thickness as in Ref. 15), which upon air exposure prevents the formation of a sufficiently homogeneous native oxide as diffusion barrier but rather leads to a complete quenching of the 2DES. Interestingly, the films of Sengupta *et al.* display a significantly lower sheet carrier density compared to our heterostructures, indicating that the exposure to air also in their samples causes a reduction of oxygen vacancies in the STO substrate, though not quite as dramatic as in our case. Unfortunately, they were not able to perform *in situ* transport measurements in order to assess the changes before and after air oxidation.

As demonstrated in Section IIIB, a thin film of disordered LAO is an excellent alternative as reliable oxygen diffusion barrier, protecting our heterostructures and their electronic interface properties from unwanted oxidation when taken *ex situ*. This is essential for reproducible device fabrication and operation. Another important aspect of d-LAO is the fact that *room-temperature* growth suffices to achieve a protecting and simultaneously electrically insulating capping, being an indispensable prerequisite for our systematic study of the role of oxygen growth pressure. Any capping material that would require higher growth temperatures will unavoidably alter the amount and distribution of oxygen and oxygen vacancies in the system in an uncontrolled way. As a consequence, this would have prevented a meaningful direct correlation between our *in situ* photoemission and *ex situ* transport data.

Other possible routes towards a surface passivation of AlO_x/STO heterostructures, including Al_2O_3 deposition by atomic layer deposition or sputtering, are viable as

long as the capping layer grows flat, blocks oxygen diffusion and is thick enough. We note in passing that a recent report on spin-charge conversion based on the AlO_x/STO heterostructure successfully used a *functional* capping, consisting of a 20 nm ferromagnetic NiFe layer covered in turn by an additional, sputtered AlO_x film [17].

We finally address the apparent lack of any systematic variation of the low-temperature mobility in our AlO_x/STO films with oxygen growth pressure. This observation seems surprising in view of the fact that in the studied O_2 pressure range the carrier density changes monotonically by more than a factor of 5 (at $T = 50\text{K}$, factor of 8 at 300 K). Naively one would expect the dual role of the oxygen vacancies in the STO substrate – controlling the sheet carrier density by *n*-doping as well as acting as scattering centers – to cause an anticorrelation between carrier concentration and mobility. However, this picture implicitly assumes that carriers and oxygen vacancies share the same vertical depth profile in the heterostructure, which in fact does not have to be the case. For example, it has recently been found that the several orders of magnitude larger mobility of the 2DES in $\gamma\text{-Al}_2\text{O}_3/\text{STO}$ with respect to that of LAO/STO results from a different density profile of the oxygen vacancies related to the specific atomic micro structure of the two interfaces [35, 36]. While the vacancies are tightly bound to the spinel-perovskite boundary of the former, they spread further out from the interface in the latter all-perovskite system. This results in a spatial separation of conduction electrons and scatterers in $\gamma\text{-Al}_2\text{O}_3/\text{STO}$ and thus its higher mobility as opposed to LAO/STO .

Against this background it seems conceivable that the oxygen vacancy distribution in our AlO_x/STO system is also affected by the structural details of the interface and, in particular, by its sensitivity to the varying oxidation conditions during Al deposition, potentially leading to a complex interplay of the different depth profiles of carriers and vacancies. The situation is further complicated by the fact that in contrast to the above-mentioned epitaxial interfaces the AlO_x films are disordered or nanocrystalline at best. For a better understanding of the transport properties it would nonetheless be desirable to determine the respective (laterally averaged) depth profiles. In principle, this information can be achieved by photoemission of the Ti *3d*-derived features in the STO-band gap, namely the metallic quasiparticle peak at the Fermi energy and the so-called in-gap peak at approx. 1.5 eV [24, 25]. While the quasiparticle peak is directly related to the mobile charge carriers, the in-gap peak probes Ti *3d* electrons locally trapped by oxygen vacancies. Measuring their angle-dependencies provides the depth profiles of carriers and oxygen vacancies, respectively, as has successfully been demonstrated for other STO-based heterostructures [35, 37]. The detection of Ti *3d*-derived interface states requires resonant photoemission at the Ti *L* edge which unfortunately has not been available for the present study but is planned for forthcoming experiments.

V. CONCLUSION

Using combined x-ray photoemission spectroscopy and transport measurements on identical samples—both *in* and, in particular, *ex situ*, the latter being enabled by the use of suitable, passivating disordered LaAlO₃ capping layers—we have demonstrated the tunability of the electronic interface properties of AlO_x/SrTiO₃ heterostructures. Upon depositing Al on the SrTiO₃ surface, oxygen is incorporated in the Al film leading to oxygen vacancies in the SrTiO₃ surface region that in turn release electrons to form a two-dimensional electron system. Its charge carrier concentration can be finely adjusted by the oxygen growth pressure, while its mobility seems to subtly depend on the detailed redox reactions, kinetics, and thermodynamics, taking place during film deposition, and thus cannot be easily controlled. Our results may be relevant for the development of device-like architectures that rely on the low-dimensional electron sys-

tems known to be inducible in SrTiO₃.

ACKNOWLEDGMENTS

The authors thank Michael Zapf for helpful discussions. We acknowledge Diamond Light Source for time on beamline I09 under proposal SI15856. The authors also thank D. McCue and D. Duncan for technical support at beamline I09.

The authors are grateful for funding support from the Deutsche Forschungsgemeinschaft (DFG, German Research Foundation) under Germany's Excellence Strategy through the Würzburg-Dresden Cluster of Excellence on Complexity and Topology in Quantum Matter ct.qmat (EXC 2147, Project ID 390858490) as well as through the Collaborative Research Center SFB 1170 ToCoTronics (Project ID 258499086).

-
- [1] A. Ohtomo and H. Y. Hwang, *Nature* **427**, 423 (2004).
 - [2] L. Li, C. Richter, J. Mannhart, and R. C. Ashoori, *Nature Physics* **7**, 762 (2011).
 - [3] A. Ohtomo, D. A. Muller, J. L. Grazul, and H. Y. Hwang, *Nature* **419**, 378 (2002).
 - [4] Y. Z. Chen, N. Bovet, F. Trier, D. V. Christensen, F. M. Qu, N. H. Andersen, T. Kasama, W. Zhang, R. Giraud, J. Dufouleur, T. S. Jespersen, J. R. Sun, A. Smith, J. Nygård, L. Lu, B. Büchner, B. G. Shen, S. Linderoth, and N. Pryds, *Nature Communications* **4**, 1 (2013).
 - [5] D. Passarello, S. G. Altendorf, J. Jeong, M. G. Samant, and S. S. P. Parkin, *Nano Letters* **16**, 5475 (2016).
 - [6] P. Schütz, D. Di Sante, L. Dudy, J. Gabel, M. Stübinger, M. Kamp, Y. Huang, M. Capone, M.-A. Husanu, V. Strocov, G. Sangiovanni, M. Sing, and R. Claessen, *Physical Review Letters* **119**, 256404 (2017).
 - [7] P. Maier, F. Hartmann, J. Gabel, M. Frank, S. Kuhn, P. Scheiderer, B. Leikert, M. Sing, L. Worschech, R. Claessen, and S. Höfling, *Applied Physics Letters* **110**, 093506 (2017).
 - [8] Y. Chen, N. Pryds, J. E. Kleibecker, G. Koster, J. Sun, E. Stamate, B. Shen, G. Rijnders, and S. Linderoth, *Nano Letters* **11**, 3774 (2011).
 - [9] W. Meevasana, P. D. C. King, R. H. He, S. K. Mo, M. Hashimoto, A. Tamai, P. Songsirittthigul, F. Baumberger, and Z. X. Shen, *Nat Mater* **10**, 114 (2011).
 - [10] L. Dudy, M. Sing, P. Scheiderer, J. D. Denlinger, P. Schütz, J. Gabel, M. Buchwald, C. Schlueter, T.-L. Lee, and R. Claessen, *Advanced Materials* **28**, 7443 (2016).
 - [11] T. C. Rödel, F. Fortuna, S. Sengupta, E. Frantzeskakis, P. L. Fèvre, F. Bertran, B. Mercey, S. Matzen, G. Agnus, T. Maroutian, P. Lecoeur, and A. F. Santander-Syro, *Advanced Materials* **28**, 1976 (2016).
 - [12] Q. Fu and T. Wagner, *The Journal of Physical Chemistry B* **109**, 11697 (2005).
 - [13] A. B. Posadas, K. J. Kormondy, W. Guo, P. Ponath, J. Geler-Kremer, T. Hadamek, and A. A. Demkov, *Journal of Applied Physics* **121**, 105302 (2017).
 - [14] L. M. Vicente-Arche, S. Mallik, M. Cosset-Cheneau, P. Noël, D. Vaz, F. Trier, T. A. Gosavi, C.-C. Lin, D. E. Nikonov, I. A. Young, A. Sander, A. Barthélémy, J.-P. Attané, L. Vila, and M. Bibes, (2021), <https://arxiv.org/abs/2102.03093>.
 - [15] S. Sengupta, E. Tisserond, F. Linez, M. Monteverde, A. Murani, T. Rödel, P. Lecoeur, T. Maroutian, C. Marrache-Kikuchi, A. F. Santander-Syro, and F. Fortuna, *Journal of Applied Physics* **124**, 213902 (2018).
 - [16] K. Wolff, R. Schäfer, M. Meffert, D. Gerthsen, R. Schneider, and D. Fuchs, *Physical Review B* **95**, 245132 (2017).
 - [17] D. C. Vaz, P. Noël, A. Johansson, B. Göbel, F. Y. Bruno, G. Singh, S. McKeown-Walker, F. Trier, L. M. Vicente-Arche, A. Sander, S. Valencia, P. Bruneel, M. Vivek, M. Gabay, N. Bergeal, F. Baumberger, H. Okuno, A. Barthélémy, A. Fert, L. Vila, I. Mertig, J.-P. Attané, and M. Bibes, *Nature Materials* **18**, 1187 (2019).
 - [18] After submission of this manuscript we became aware of [14] also addressing this issue.
 - [19] M. Kawasaki, K. Takahashi, T. Maeda, R. Tsuchiya, M. Shinohara, O. Ishiyama, T. Yonezawa, M. Yoshimoto, and H. Koinuma, *Science* **266**, 1540 (1994).
 - [20] G. Koster, B. L. Kropman, G. J. H. M. Rijnders, D. H. A. Blank, and H. Rogalla, *Applied Physics Letters* **73**, 2920 (1998).
 - [21] A. V. Naumkin, A. Kraut-Vass, C. J. Powell, S. W. Gaarenstroom, and National Institute of Standards and Technology (U.S.), NIST X-ray photoelectron spectroscopy database (2012).
 - [22] K. Eom, E. Choi, M. Choi, S. Han, H. Zhou, and J. Lee, *The Journal of Physical Chemistry Letters* **8**, 3500 (2017), publisher: American Chemical Society.
 - [23] M. Sing, G. Berner, K. Goß, A. Müller, A. Ruff, A. Wetscherek, S. Thiel, J. Mannhart, S. A. Pauli, C. W. Schneider, P. R. Willmott, M. Gorgoi, F. Schäfers, and R. Claessen, *Physical Review Letters* **102**, 176805 (2009).
 - [24] G. Berner, M. Sing, H. Fujiwara, A. Yasui, Y. Saitoh, A. Yamasaki, Y. Nishitani, A. Sekiyama, N. Pavlenko, T. Kopp, C. Richter, J. Mannhart, S. Suga, and R. Claessen, *Physical Review Letters* **110**, 247601 (2013).

- [25] J. Gabel, M. Zapf, P. Scheiderer, P. Schütz, L. Dudy, M. Stübinger, C. Schlueter, T.-L. Lee, M. Sing, and R. Claessen, *Physical Review B* **95**, 195109 (2017).
- [26] P. Scheiderer, F. Pfaff, J. Gabel, M. Kamp, M. Sing, and R. Claessen, *Physical Review B* **92**, 195422 (2015).
- [27] R. Revie and H. Uhlig, *Corrosion and Corrosion Control - An Introduction to Corrosion Science and Engineering*, 4th ed. (John Wiley & Sons, New York, 2008).
- [28] A. Sambri, D. V. Cristensen, F. Trier, Y. Z. Chen, S. Amoruso, N. Pryds, R. Bruzzese, and X. Wang, *Applied Physics Letters* **100**, 231605 (2012).
- [29] A. Joshua, S. Pecker, J. Ruhman, E. Altman, and S. Ilani, *Nature Communications* **3**, 1129 (2012).
- [30] See Supplemental Material at [URL will be inserted by publisher], section II, for a detailed discussion of the Hall effect measurement and analysis process. .,
- [31] F. Trier, K. V. Reich, D. V. Christensen, Y. Zhang, H. L. Tuller, Y. Chen, B. I. Shklovskii, and N. Pryds, *Applied Physics Letters* **111**, 092106 (2017).
- [32] S. Raghavan, J. Y. Zhang, and S. Stemmer, *Applied Physics Letters* **106**, 132104 (2015).
- [33] G. L. Yuan and A. Uedono, *Applied Physics Letters* **94**, 132905 (2009).
- [34] B. Veličkov, V. Kahlenberg, R. Bertram, and M. Bernhagen, *Zeitschrift für Kristallographie* **222**, 466 (2009).
- [35] P. Schütz, D. Christensen, V. Borisov, F. Pfaff, P. Scheiderer, L. Dudy, M. Zapf, J. Gabel, Y. Chen, N. Pryds, V. Rogalev, V. Strocov, C. Schlueter, T.-L. Lee, H. Jeschke, R. Valenti, M. Sing, and R. Claessen, *Physical Review B* **96**, 161409(R) (2017).
- [36] D. Christensen, V. Y. Frenkel, P. Schütz, F. Trier, S. Wissberg, R. Claessen, B. Kalisky, A. Smith, Y. Z. Chen, and N. Pryds, *Physical Review Applied* **9**, 054004 (2018).
- [37] C. Cancellieri, M. L. Reinle-Schmitt, M. Kobayashi, V. N. Strocov, T. Schmitt, P. R. Willmott, S. Gariglio, and J.-M. Triscone, *Phys. Rev. Lett.* **110**, 137601 (2013).